Study of radiotherapy treatment for lung cancer and its dose calculation

Abstract

Background: Lung cancer is one of the leading causes of morbidity and mortality around the world, so effective treatment methods are necessary. The aim of this study was to investigate the lung cancer treatment by radiotherapy, and the dose changes to lung inhomogeneity density.

Materials and Methods: The technique employed in this study was separated into two sections. For configurations and procedures in the first portion, a computerized care planning system was employed. After the primary data from the system has been corrected, phase two of the configuration was utilized to obtain experimental results using a container for ionization as a baseline. This study included treatment planning that involves highly specialized treatment for lung cancer and the shift in variance of the dosage administered, as the density of the lungs constantly changes. Collapsed Cone Convolution Superposition (CCCS) has been used to help in evaluation of lung dose calculation approaches in relation to relative lung density, treatment geometry, and dosage comparisons.

Results: The outcome of this study suggests that homogeneous CCCS portions are within 1% of the adaptive convolution (AC) doses, implying that the AC, which benefits from faster processing times, is a good alternative for the CCCS.

Conclusion: Dose absorption that is calculated by utilizing the TPS is based on the CCCS algorithm that provides an accurate result with the help of Monte Carlo

Calculations under the circumstances of the heterogeneous media and low-density materials like the lungs.

Keywords: lung cancer, small cell lung cancer, non-small cell lung cancer, radiotherapy, Dose Calculation, heterogeneous media, low-density materials.

1. Introduction

Lung cancer occurs when there is an abnormal growth of cells that cluster together in the lungs and they also affect the healthy lung tissues around them [1]. This type of cancer has the highest incidence in men [2], it is also the leading cause of cancer death in men and women around the world [3].

Among other cancers, Lung cancer has been ranked first worldwide, its highest incidence rate 13% was noted in 2012 and increased by around 18% in 2015 [2]. In Australia, lung cancer became among the highest four types of cancer to be diagnosed in 2007. About 5,948 males and 3,755 females were diagnosed with lung cancer during that year [4].

Smoking is the major risk factor of lung cancer, both as active smokers and passive smokers, since cigarette causes about 80% of lung cancer cases [2]. Other risk factors of lung cancer include; air pollution, chemicals (paint materials, chemical waste, asbestos, radon), unhealthy food (containing polycyclic aromatic hydrocarbons, such as junk food and satay), jobs that lead to carcinogen exposure (painters, construction workers, drivers), alcohol (>30g/day), family history of cancer, a history of pulmonary disease (tuberculosis, asthma), and lack of physical activity [5,6].

Lung cancer is divided into two types; small cell lung cancer (SCLC) and non-small cell lung cancer (NSCLC) [1,7,8]. Depending on their clinical course, SCLC and

NSCLC should be seen as two different diseases [7]. Studies show that over 86% of cases of lung cancer are NSCLC [1, 8]. NSCLC has a slow growth rate compared to SCLC. Usually, the slow growth rate is dangerous because few or no symptoms can be recognized until advanced stages. The three main types of NSCLC include squamous cell, large-cell undifferentiated carcinoma, and adenocarcinoma of the lung [9].

The treatment of lung cancer is usually complicated, and involve multiple treatment modalities including; surgery, systemic therapies (targeted agents, chemotherapy and immunotherapy), radiotherapy, palliative care and interventional radiology [10]. Despite rapid development in treatment technology and the additional options of treatment for this aggressive cancer, survival still poor, particularly in metastatic and locally advanced lung cancer [3].

Radiotherapy is the only treatment modality for which there are indications in all stages of disease and across all categories of patient performance status [10]. The thorax remains a challenging anatomical site for radiotherapy, because of respiratory- and cardiac-induced tumor motion, the low electron density of lung and the closeness of critical structures such as the spinal cord and esophagus. However, advanced radiotherapy technologies can address many of these challenges [11], resulting in improved outcomes in lung cancer treatment [10]. However, radiotherapy still underutilized in many parts around the world [10].

Radiation oncology is medical specialty has very high Medicare expenditures, therefore the clinical benefit of such technology still needs to be demonstrated [12]. Hence this study aimed to investigate the lung cancer treatment with radiotherapy, and the dose changes to lung inhomogeneity density.

2. Material and Methods

The technique employed in this study was separated into two sections. For configurations and procedures in the first portion, a computerized care planning system was employed. After the primary data from the system has been corrected, phase two of the configuration was utilized to obtain experimental results using a container for ionization as a baseline.

2.1 Procedure for the TPS which is (Computerized Treatment Planning System)

Figure (1) depicts the Philips Healthcare's Pinnacle 3 treatment planning framework in the Netherlands, which is intended to acquire data for the computerized treatment planning framework. The Pinnacle3 software used in this study is owned by the University of Wollongong.

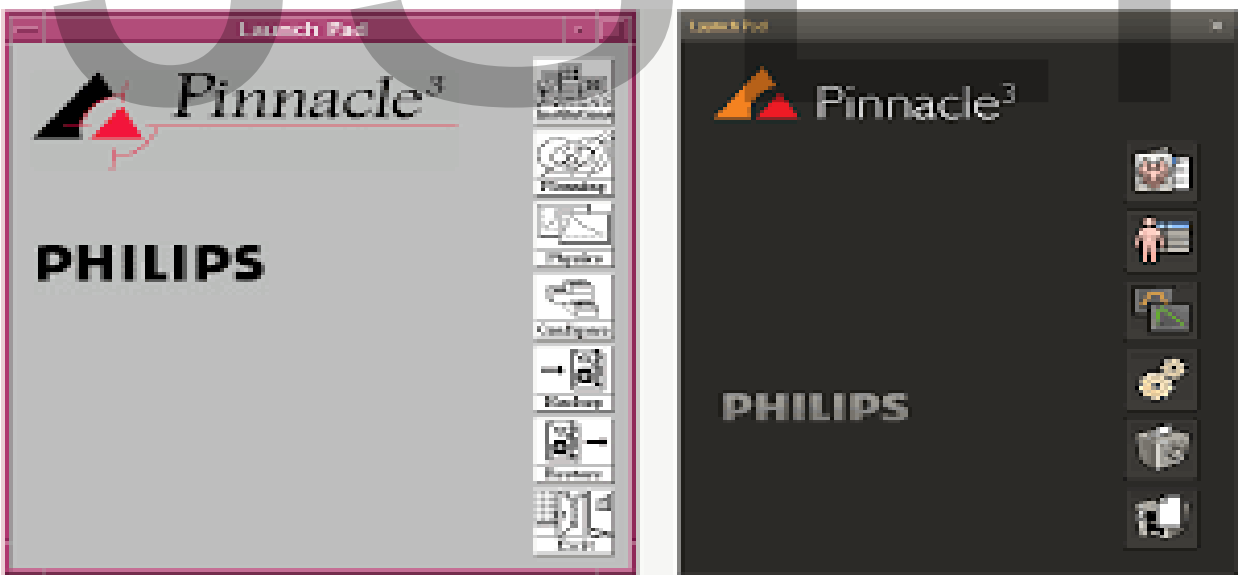

Figure 1: Pinnacle3 Employed in This Research

The dosage grid was expanded to encompass the entire area width and depth, both of which are set to 25 cm, and the granularity of the dosing matrix is fixed to 2mm. It's

established that the dose is estimated properly between matrix nodes for both narrower and wider gaps, since if insinuate estimation isn't done correctly, the dose would be erroneous, particularly in penumbra sections, build u regions, and interfaces. As a result, an acceptable number should be selected at the commencement of the grid size specification, and the results should be evaluated to ensure that the grid dimension is operating right.

Using grid spacing that is continuous and/or irregular it’s also critical to optimize the interpolation approach for determining dose between grid points and align the coordinate system where the dose computation sites are designated in both the picture and machine coordinate systems.

The phantom is made up of three areas. They also have a total penetration distance of 25cm. The first section (POI1) has a density of 1 g/cm3 and a depth of 5 cm. The density of the second region (i.e., the lung phantom) might differ, but it usually ranges between 5 and 15 cm deep. The depth of the third area (POI3) can range from 20 to 25 centimeters. According to the ECWG measurement values, two radiation intensities were used in in this study 6MV and 10MV in the SSD (source to surface distance) at 100 cm. The SSD plays a critical role in estimating the dosage dissemination and yield element for electron radiations.

Field sizes range from 3cm x 3cm to 5cm x 5cm to 10cm x 10cm. Because of the tight association between field size and radiation dosage, determining the relevant patient portions gets achievable.

0.1 gm/cm3, 0.2 gm/cm3, 0.3 gm/cm3, and 0.4 gm/cm3 were the numerous amounts utilized to experiment with the density of the phantom for examining the impacts of

density variation. The mass attenuation and absorption coefficients show how photons are affected by their mass density. As a result, there is a high correlation between dosage computation and the density of the media that will be irradiated. In addition, the three various field widths were treated to a radiation of 6 MV energy, and simulation of the four distinct densities was done with 10 MV - all of this occurred concurrently. The essential setups in this assignment should be stored for part two processes. Multiple data sets for field sizes, as well as varied lung densities, were collected as a component of this operation. Using the same data analysis, the tolerance between the real experimentally determined standard values and the Pinnacle3 generated simulation was contrasted.

2.2 Experimental Procedure

All the layouts from the first phase are still available. The configuration of the tests in Wollongong Hospital, which used the Varian 21Ex Linear Accelerator (Linac), can be shown in Figure (2). Furthermore, ionization chambers were used to detect dosage fluctuations in these investigations.

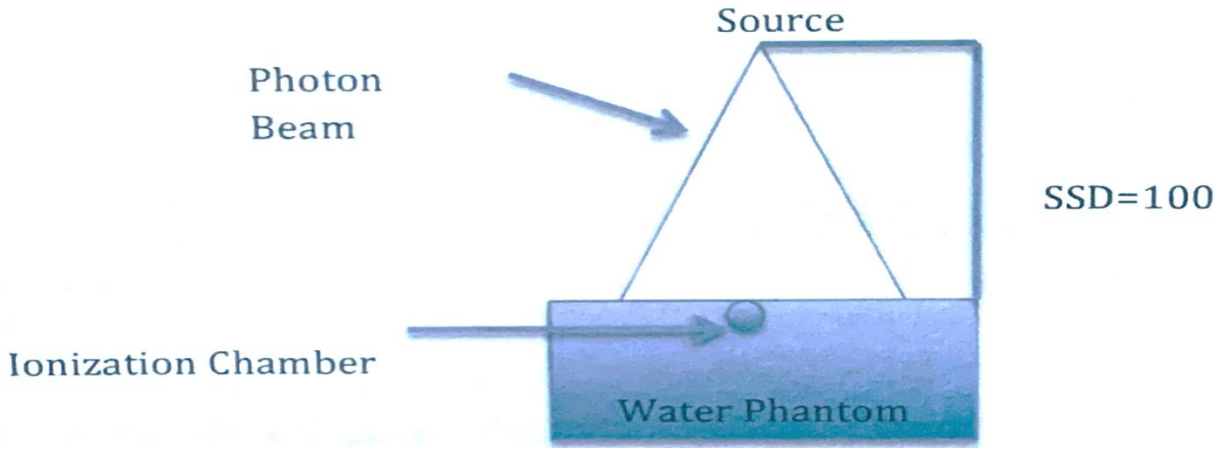

Figure 2 the experimental setup for initial measurement.

It is required to perform several preliminary procedures to ensure that the LINAC settings meet the treatment requirements. The first action is to double-check the collimator rotation to ensure that it has a 1mm run out. Similarly, it is crucial to assess the gantry rotation to ensure that the run-out is less than ±1 mm off the standard. Thereafter, check to see if the table rotation has a ±1mm run out from the baseline. An additional criterion is that the laser alignment tolerance is less than 1 millimeter. As a result, we've verified the LINAC's maximum efficiency, and these evaluations was used as standard settings for the commissioning process. The solid water phantom must be in the isocenter in the second stage. The mid-point of the measuring ionization chamber should be established with the isocenter and a standard SSD (of 100cm dimension). In addition, each size should be normalized to a certain depth.

Furthermore, it is suggested that the referencing ionization chamber be placed at various desired locations and under the field size. The solid water phantom is made up of several sections, one of which has a whole figure (3). By moving this piece along the phantom, you can choose from a variety of depths. As a result, the ionization chamber was allowed to penetrate the solid water phantom through this opening. These inspections verify that the measuring setup is precise and that it can act as standardized settings for gathering reliable data, with the foundation being the commissioning processes.

Figure 3 shows the initial evaluation setup utilizing an ionization chamber.

A CC04 conventional ionization chamber is shown in Figure 4. This ionization chamber was used in studies looking at the ling reciprocal dose in radiotherapy. In a heterogeneous lung phantom, this ionization chamber was also used to measure the central axis absorbed dose. A robust apparition of "water" with a minimal density of lung P=0.3g/cm3 and a measure of water density P=1g/cm3 was used. For obtaining the depth, a range of distances was examined, and 6MV and 10MV of energy were used. Three distinct field dimensions are used in this research: 3cm x 3cm, 5cm x 5cm, and 10cm x 10cm. Employing the ionization chamber technique as a reference, we investigated how precise, in the treatment planning paradigm's viewpoint, the amount of dosage (Pinnacle3).

Figure 4 the Ionisation chamber (CC04)

2.3 Methods of Dose Calculation

The 3D treatment planning framework Pinnacle3 was employed in this investigation. Furthermore, a (CCCS) algorithm was used to determine the lung apparition dosage distribution.

A true three-dimensional dose estimate is acquired by the helping of the CCCS dose model, which considers primary photon incidence and secondary electrons, as well as heterogeneity difficulties in lung regions. The dose distribution in components functioning on which there may be an electronic imbalance, such as the air cavity in the lungs, can be determined utilizing the CCCS approach. The CCCS dosage model satisfies the treatment planning system's major aims of reliable determination and low time cost.

2.3.1 Convolution Superposition Dose Model

The Mackie et al method served as the foundation for Pinnacle3's CCCS dosage algorithm framework. The CCCS algorithm does not use correction factors to

improve dose allocation estimations; instead, it uses first-principles computations to determine dose distributions. It may now consider the effects of inhomogeneous tissue, exterior patient contours, and radiation modulator on dose allocation [13].

The follow method is essential for the start of the CCCS dosage algorithm. The incident photons must first be modularized, with the source being the accelerator's head. As the patient's sample density in the projection is intersected by this energy penetr, the second stage is estimating the TERMA (Total energy Released per unit Mass) volume. The ray-tracking method is used to monitor lateral scatter including the influence of heterogeneities across the TERMA's energy implantation kernel in three-dimensional conjunction. Eventually, although the electrons severely fall abruptly and have been medialized, we contaminate the estimated photon dosage allocation.

2.3.2 Adaptive Convolution Superposition

Pinnacle3 similarly employs the adaptive convolution superposition (ACS) approach, however with some modifications to the computation methods. The TERMA was evaluated in conjunction with a coarse 3D grid with dose distribution. Regarding the top portion of curvature, the computer delivers a high-resolution dose allocation at the intermediate stage. After that, the computer improves the resolution change in the higher curvature area dynamically. With that being said, the resolution must be great enough to be taken into consideration for this. The coarse dose grid is where the dose distribution enters from in the case of the lower curvature area. Under the influence of the adaptive convolution superposition (ACS) method, the computation time is decreased and the CCCS calculation is not made any less accurate from the heterogeneities of the tissues as well.

PDF-XChange Editor Click to BUY NOW! www.tracker-software.com

3. Results

Findings from the Treatment Planning System Pinnacle3 were analyzed utilizing CCCS computations to look at the influence of density variation for various irradiation intensities and field dimensions.

3.1 Depth-dose characteristics for a diverse apparition at 6 and 10 MV and different area dimensions in varied lung apparition concretions

The proportion of comparative dosage versus depth in cm is shown in next figures. Water with a concretion of 1 g/cm3 was utilized to approximate the density of the human body from the phantom's surface to a depth of 5 cm. The chart comprises of various curves, between 5 cm and 15 cm (for depth) portray lungs of varying densities with densities ranging from 0.1, 0.2, 0.3, and 0.4 g/cm3. The additional depth between 15 cm and 25 cm represent the periphery of the human body, which is made up mostly of water with a concretion of 1 g/cm3.

The answer in the curve was obtained by using a radiation intensity of 6MV and field dimensions of 3 cm x 3 cm for the evaluation. As can be seen from the figure 5, the relative percentage of absorbed dosage falls as depth rises. When opposed to the water media, the percentage of reduction was larger in the medium with lower density, which is the lung. The lesser the density, the lesser the proportional dose, and 0.1 g/cm3 had the lowest proportional dose, according to the graph. The 0.2 g/cm3 was accompanied by a 0.3 g/cm3 and 0.4 g/cm3, however, the 0.3 g/cm3 and 0.4 g/cm3

showed a slight change in absorption slope when opposed to the two-water media.

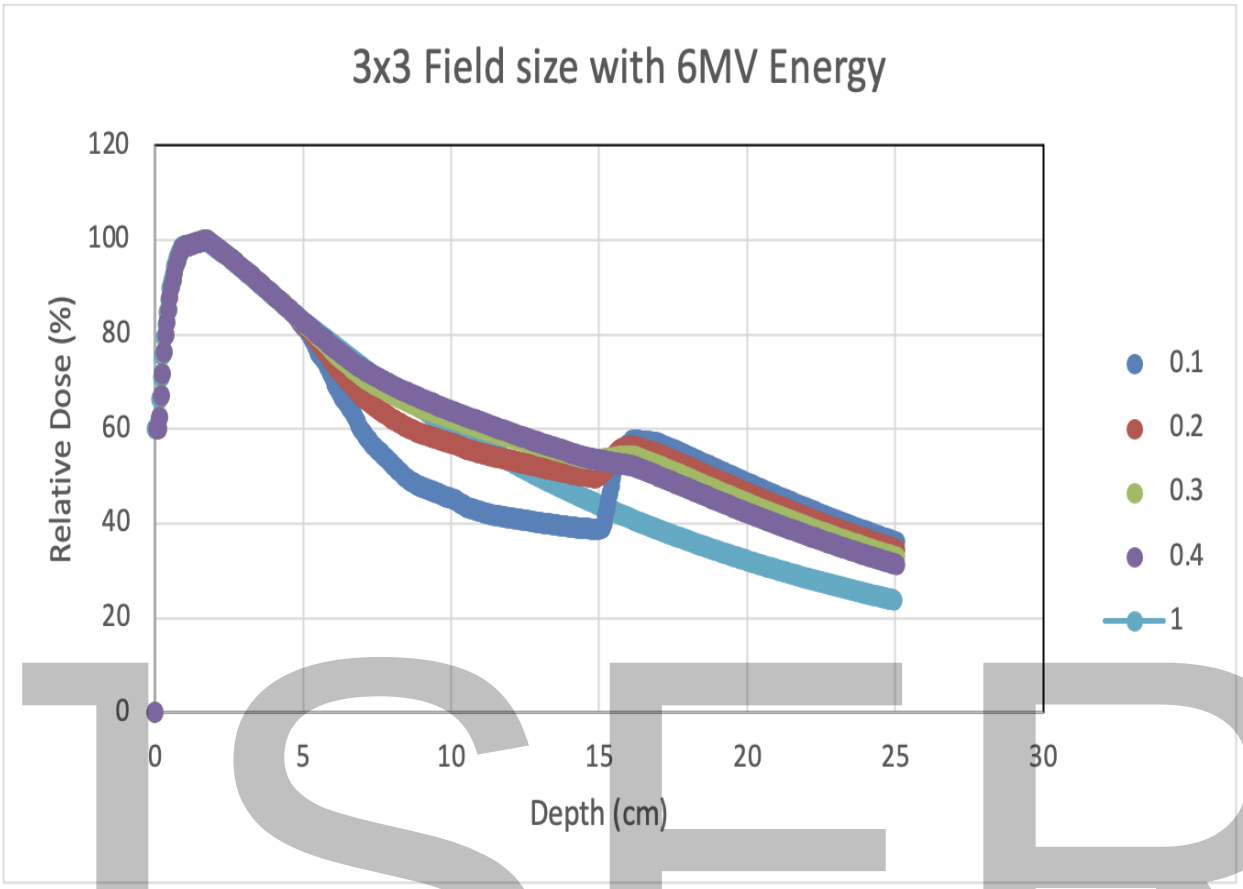

Figure 5: A composite apparition's depth-dose characteristics at 6MV and a field dimension of 3cmx3cm in varied lung apparition densities (0.1, 0.2, 0.3, and 0.4) g/cm3.

Next figure (6) shows the depth-dose characteristics for a diverse apparition at 6MV with a 5cmx5cm area dimension at various lung apparition concretions. The tendency in water media with 1 g/cm3 stays identical for the 6MV with 5 x 5 cm area dimension as for the 3 x 3 field dimension with 6MV radiation intensity delivery. One variation is the change is in the lung medium, which was more visible with the 0.1 g/cm3 in this instance.

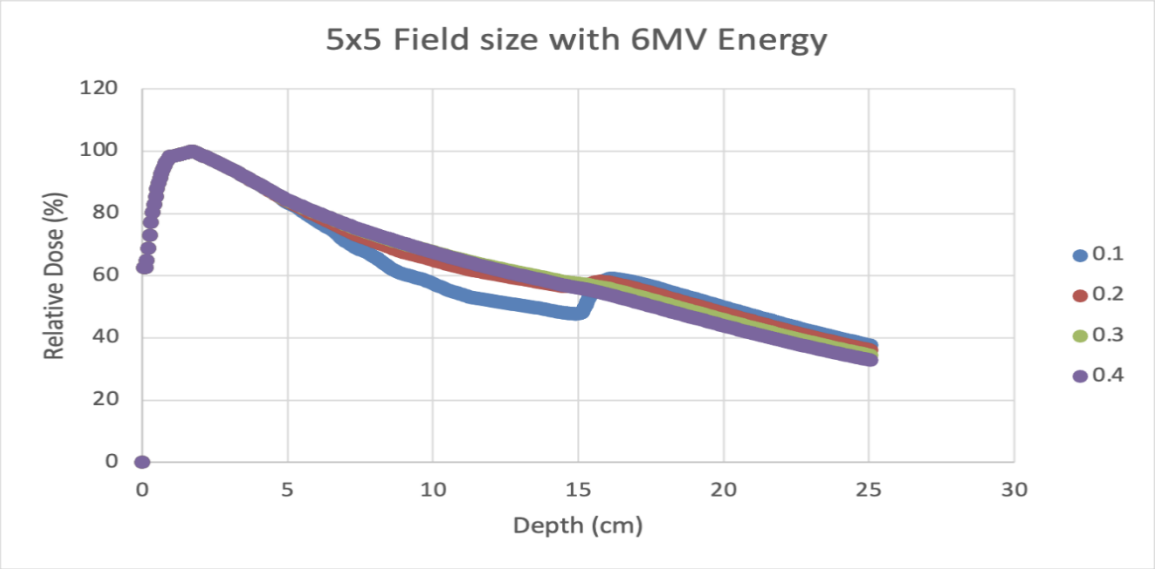

Figure 6: Depth-dose characteristics for a diverse apparition at 6MV with a 5cmx5cm area dimension at various lung apparition concretions (0.1, 0.2, 0.3, and 0.4) g/cm3.

Figure 7 shows the depth-dose characteristics for a diverse apparition at 6MV with area dimension of 10cmx10cm in varied lung apparition concretions (0.1, 0.2, 0.3, and 0.4) g/cm3. It is clear that in the lung medium, the density has no significant shift with a field dimension of 10 cm x 10 cm and the same radiation intensity delivery of 6MV.

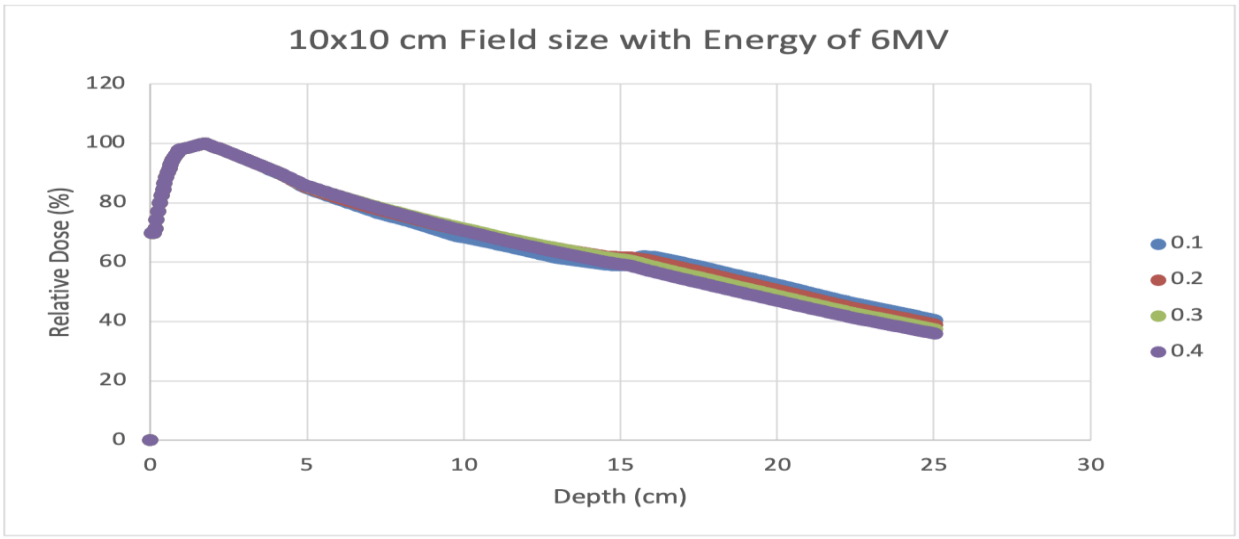

Figure 7: Depth-dose characteristics for a diverse apparition at 6MV and an area dimension of 10cmx10cm in varied lung apparition concretions.

Next figure shows the depth-dose characteristics for a diverse apparition at 10MV and an area dimension of 3cmx3cm in varied lung apparition concretions (0.1, 0.2, 0.3, and 0.4) g/cm3. For the 0.1 g/cm3 density, the lung medium revealed a considerable decrease in absorption. The 0.3 g/cm3 and 0.4 g/cm3 values were absent from the lung and lower body (water) mediums.

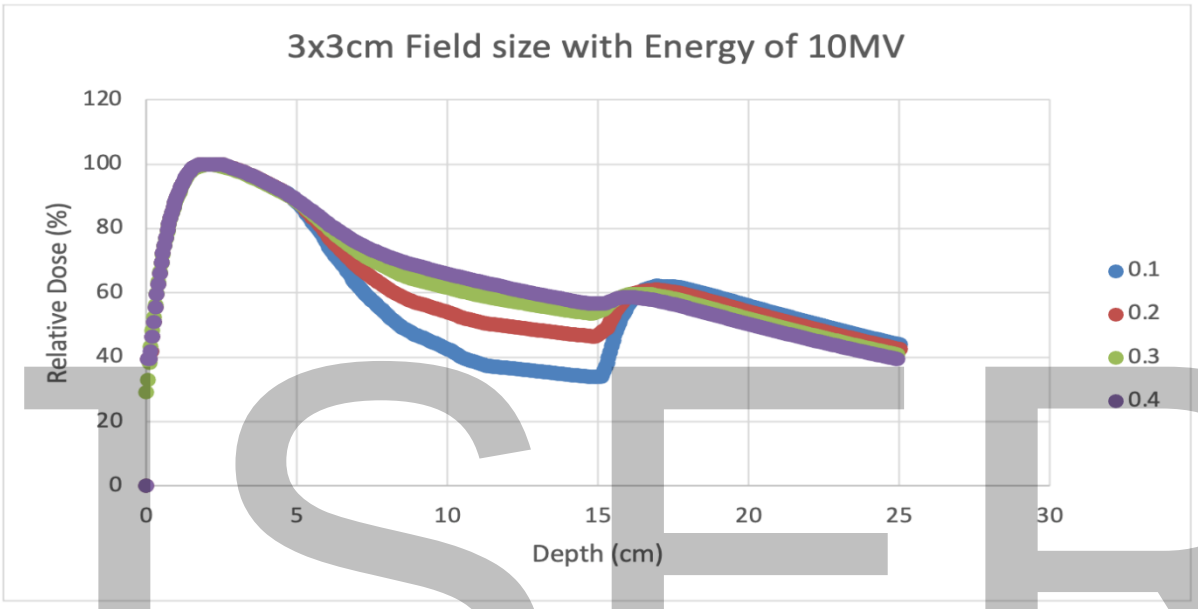

Figure 8: Depth-dose characteristics for a diverse apparition at 10MV and an area dimension of 3cmx3cm in varied lung apparition concretions.

Figure 9 shows the depth-dose characteristics for a diverse apparition at 10MV and an area dimension of 5cmx5cm in varied lung apparition concretions (0.1, 0.2, 0.3, and 0.4) g/cm3. it is clear that There was a decreased percentage of absorption at concretions of 0.1 g/cm3 and 0.2 g/cm3 in the lung media. For densities of 0.3 g/cm3 and 0.4 g/cm3, the difference in absorption ratio was not noticeable.

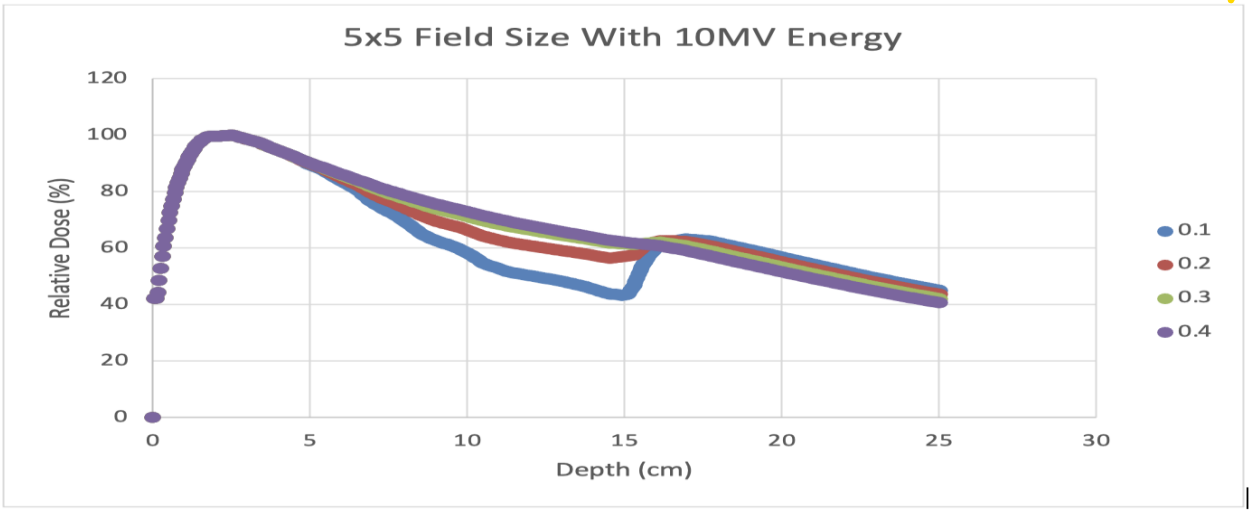

Figure 9 : Depth-dose characteristics for a diverse apparition at 10MV and an area dimension of 5cmx5cm in varied lung apparition concretions.

According to figure 10; the radiation energy of 10 MV was delivered to a field dimension of 10 cm × 10 cm in figure 10. Excluding the 0.1 g/cm3 in the lung media, at which the percentage of absorption was reduced, there is a general pattern in the absorption ratio for the densities.

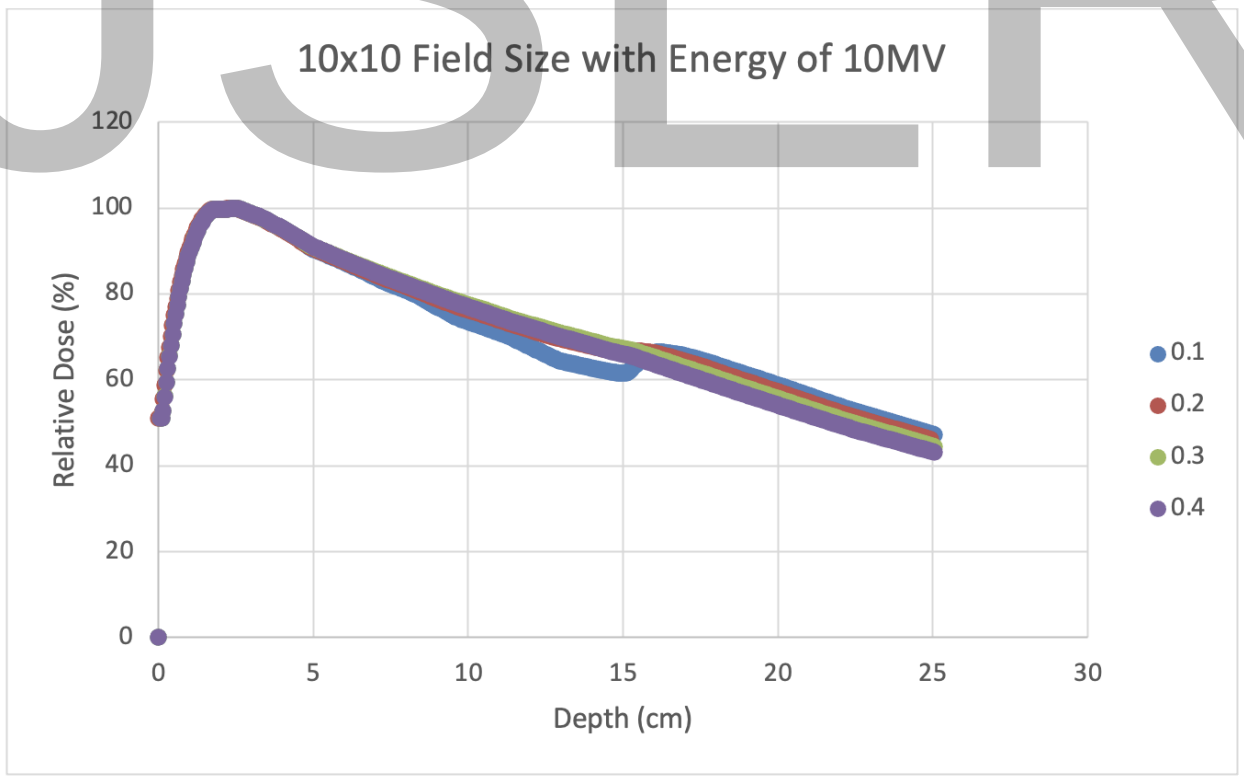

Figure 10: Depth-dose characteristics for a diverse apparition at 10MV and an area dimension of 10cmx10cm in varied lung apparition concretions.

3.2 As benchmark, the different results of ICM which is Ionisation Chamber Measurement and TPS CCCS. Using TPS CCCS and Ionization Box Assessment as a baseline and contrast the findings.

For this phase of the correlation, the arithmetic means of the concretions utilized in Pinnacle3 was selected and determined to be 0.3 g/cm3. For the present study, a 5% precision margin was put into account.

In figure 11 The findings were contrasted using a heterogeneous phantom with a density of 0.3 g/cm3 as an average density inside the lung media and beam intensity of 6MV bombarded through a 3 cm x 3 cm field dimension. Throughout all depths, the graph revealed concordance between pinnacle3 and the ionization container.

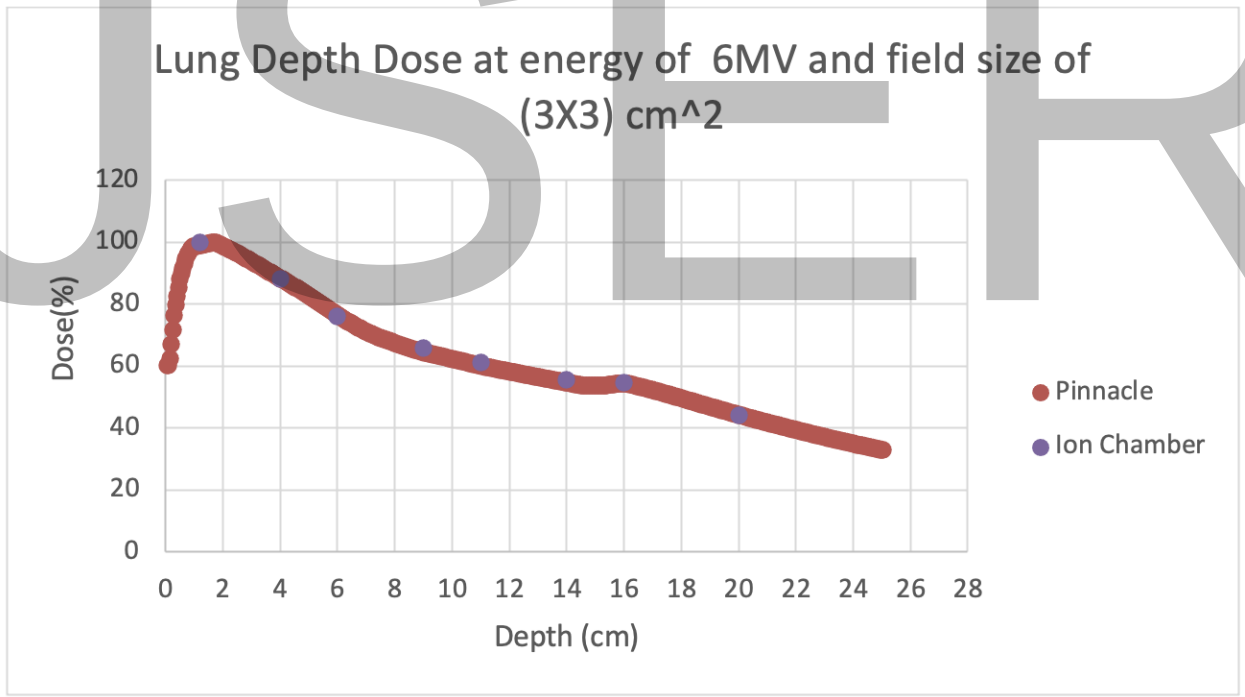

Figure 11; comparison findings from the benchmark ionization chamber and the treatment planning simulation Pinnacle3 CCCS, at the identical radiation energy of 6MV and the same field dimension of 3cmx3cm

Next figure shows the comparing between findings from the benchmark ionization chamber and the treatment planning simulation Pinnacle3 CCCS, at the identical radiation energy of 6MV and the same field dimension of 5cmx5cm. The observed and calculated findings are shown in figure 12, although in this instance, a 6MV energy radiation was radiated via a field dimension of 5 cm x 5 cm. For the heterogeneous phantom, an average density of 0.3 g/cm3 was achieved. Throughout all depths, the graph indicated consistency between pinnacle3 and the ionization chamber.

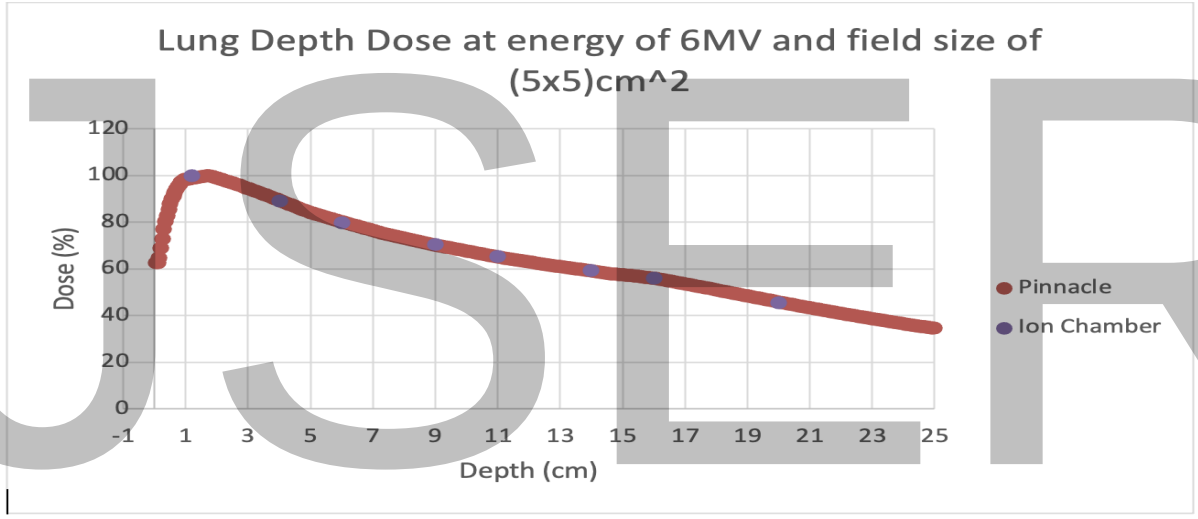

Figure 12 comparison the findings from the benchmark ionization chamber and the treatment planning simulation Pinnacle3 CCCS, at the identical radiation energy of 6MV and the same field dimension of 5cmx5cm.

The estimated and observed findings for the identical condition of 0.3 g/cm3 density for diverse apparition, radiation intensity of 6MV, and area dimension of 10 cm × 10 cm were contrasted in figure 13. The estimated dose when the CCCS computation technique was applied was well within the ionization chamber's standard error at every depth of observation, according to the results of this study.

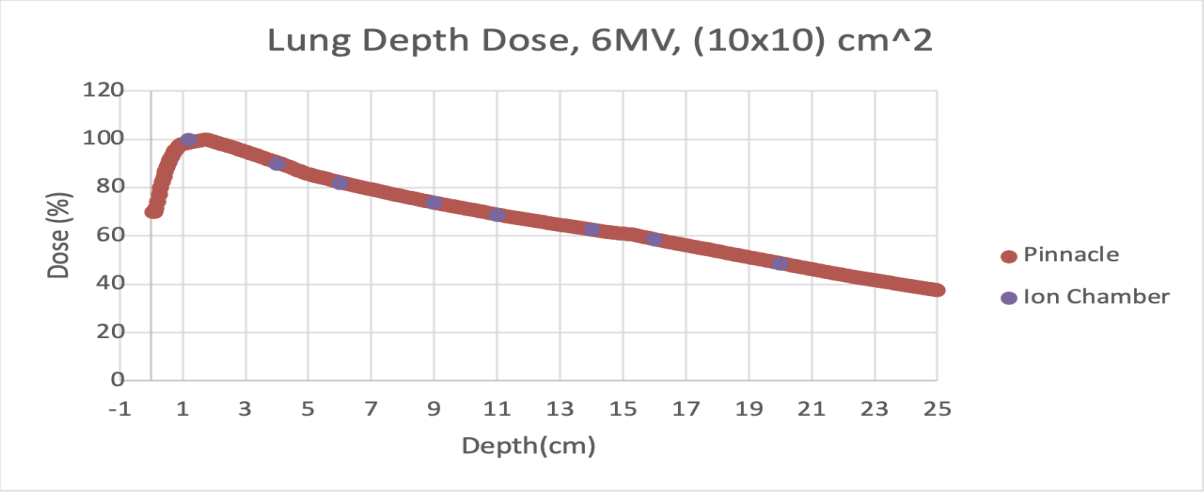

Figure 13 at the identical radiation energy of 6MV and the same field dimension of 10cmx10cm, the findings from the benchmark ionization chamber and the treatment planning simulation Pinnacle3 CCCS were compared.

The calculated and observed findings for the identical circumstance of 0.3 g/cm3 density for heterogeneous phantom, beam intensity of 10MV, and field dimension of 3 cm x 3 cm were contrasted in Figure 14. The results of pinnacle3 and the ionization box for the phantom at a heterogeneous low-density media were subtly different from one another, as indicated in the graph. As a corollary, there is a minor discrepancy between the pinnacle3 findings and the ionization chamber findings.

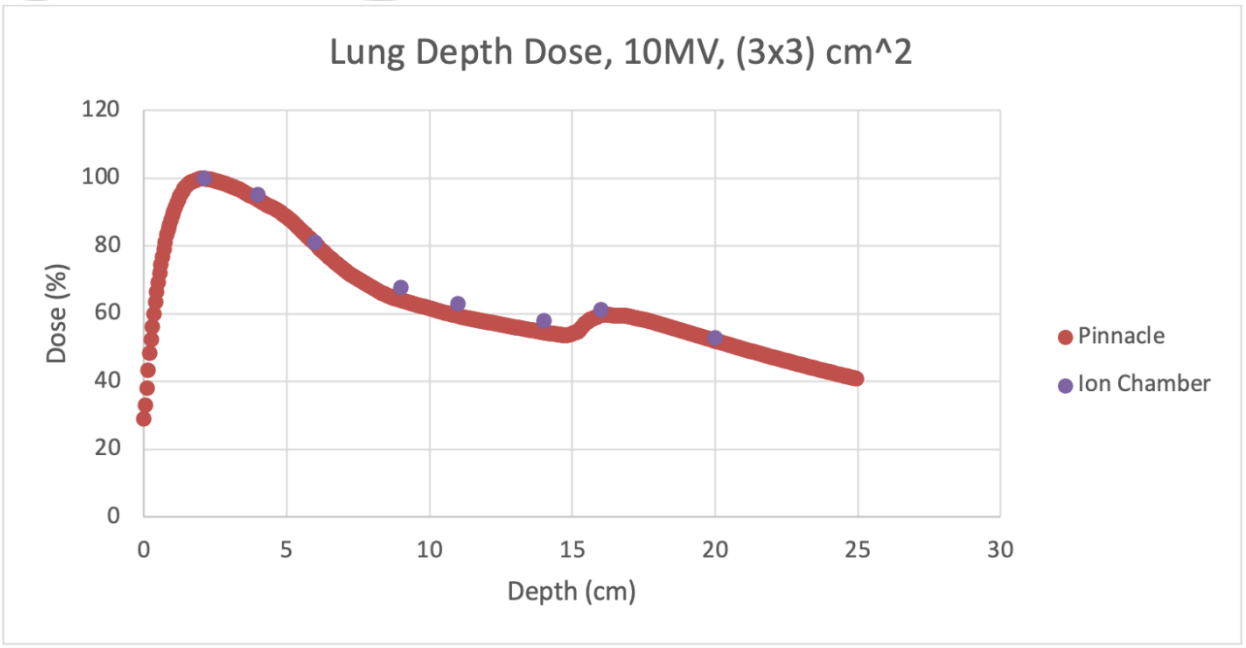

Figure 14 at the identical radiation energy of 10MV and the same field dimension of 3cmx3cm, the findings from the reference ionization chamber and the treatment planning simulation Pinnacle3 CCCS were compared.

As per figure 15, the low-density media agrees with the CCCS assessment at all levels, excluding 14cm and 16cm depths, where there is a little inaccuracy since the observed result was marginally greater than the CCCS simulation findings. Even though this test was carried out with a 10 MV beam intensity, a field dimension of 5 cm x 5 cm, and 0.3 g/cm3 of heterogeneous material.

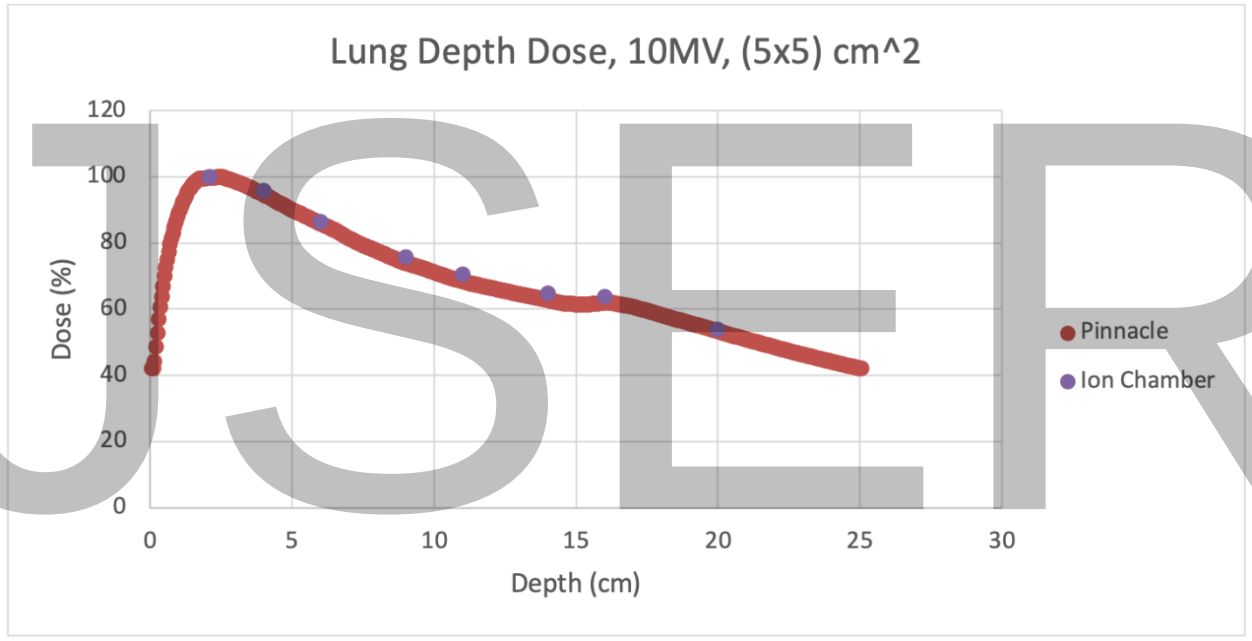

In the Figure 15 comparison of the results gained from the standard benchmark ionisation chamber and the treatment planning simulation Pinnacle^3 CCCS for the beam energy 10MV with the field size being at 5cm x 5cm are made.

Figure 16 depicts the comparison between the results of the ionization container and the CCCS simulation using 10MV of beam intensity delivered through a field dimension of 10 cm x 10 cm. Throughout all depths, there was concordance between pinnacle3 and the ionization compartment.

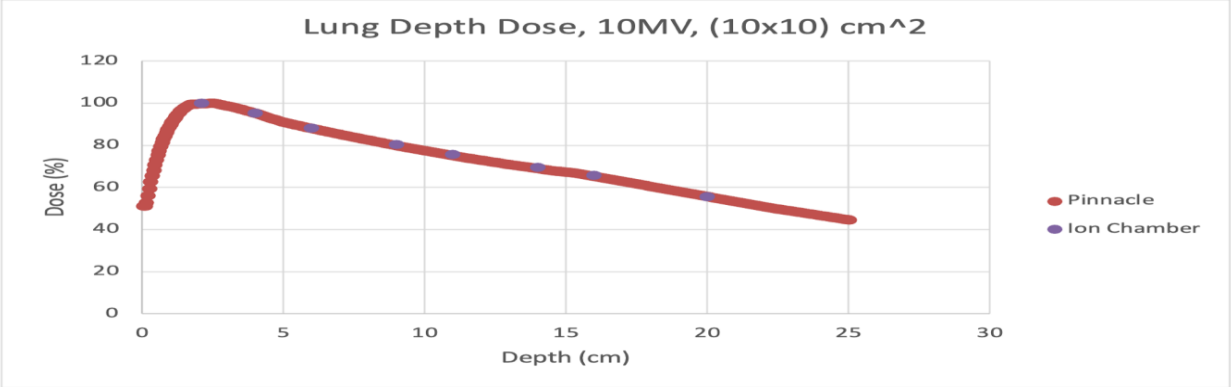

In figures 16, comparison the results gotten from the benchmark ionisation chamber and treatment planning simulation Pinnacle^3 CCCS for the beam energy of 10MV and a field size 10cmx10cm.

3.3 Curves of Isodose Comparison

In figures 17, the comparison between the isodose curves at the same beam energy of 6MV and heterogeneous density of 0.3 g/cm3 was made but at different field sizes that are at 3x3 cm, 5x5 cm, and 10x10 cm. A symmetrical dose profile for all field sizes was seen. The curve residing over the penumbra region remained smooth. At the edges of the field sizes 3x3 cm and 5x5 cm, the flatness of the profile was lost. The overall variation in the penumbra was about 5% which is small. Finally, the differences between the ORA% of 3x3 cm and 5x5 cm was on the smaller side of about 20%.

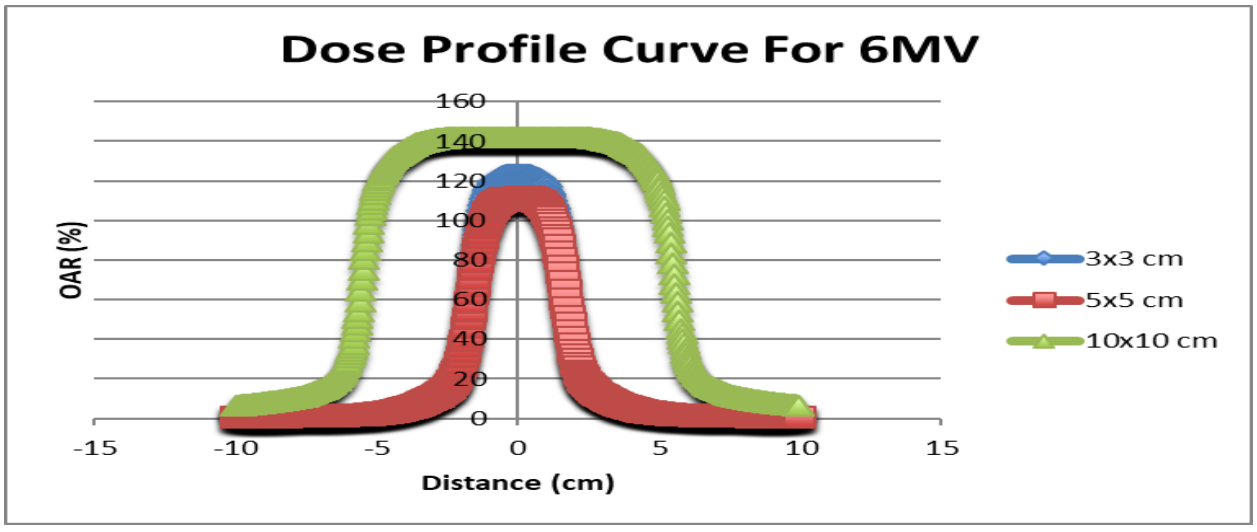

figures 17 Isodose curves gained at the beam energy of 6MV for 3 cm x 3 cm, 5 cm x 5 cm and 10 cm x 10 cm at a density of 0.3 g/cm^3 are given in the figure 4-13

In figures 18, the same beam energy of 10 MV was used for field sizes 3x3 cm, 5x5 cm, and 10x10 cm for the development of the dose profile curve that is seen. A Heterogeneous density of 0.3 g/cm3 was used and was kept as a constant. Overall, the penumbra region was found to be smooth, but the flatness of the profile was found to be lost for only the 10x10 cm field size. A symmetrical dose profile was about the Y-axis for the three different field sizes discussed. The variation profile seen in penumbra is small and about 10% and the difference in ORA% between 3x3 cm and 5x5 cm was bigger, at about 40%.

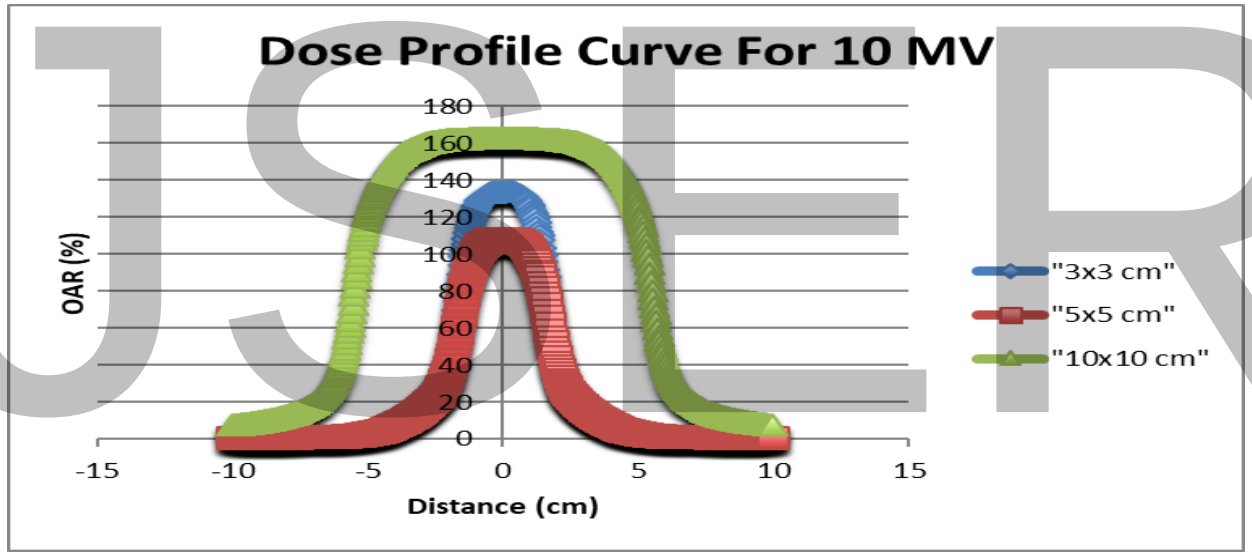

Figure 18 Isodose curves for the beam energy of 10MV for the field size 3 cm x 3 cm, field size 5 cm x 5 cm and field size 10 cm x 10 cm at a density of 0.3 g/cm^3.

3.4 The Influence of Field Size

As seen in figure 19, For the irradiation of field sizes 3x3 cm, 5x5 cm, and finally the 10x10 cm a6MV beam of energy was used. The lung medium with a heterogeneous density of 0.3 g/cm3 was between a depth of 5 cm and 15 cm. insignificant changes in absorbed doses were seen in the 10x10 cm and 5x5cm field sizes. Finally, there was a small change in absorbed dose for the field size of 3x3 cm.

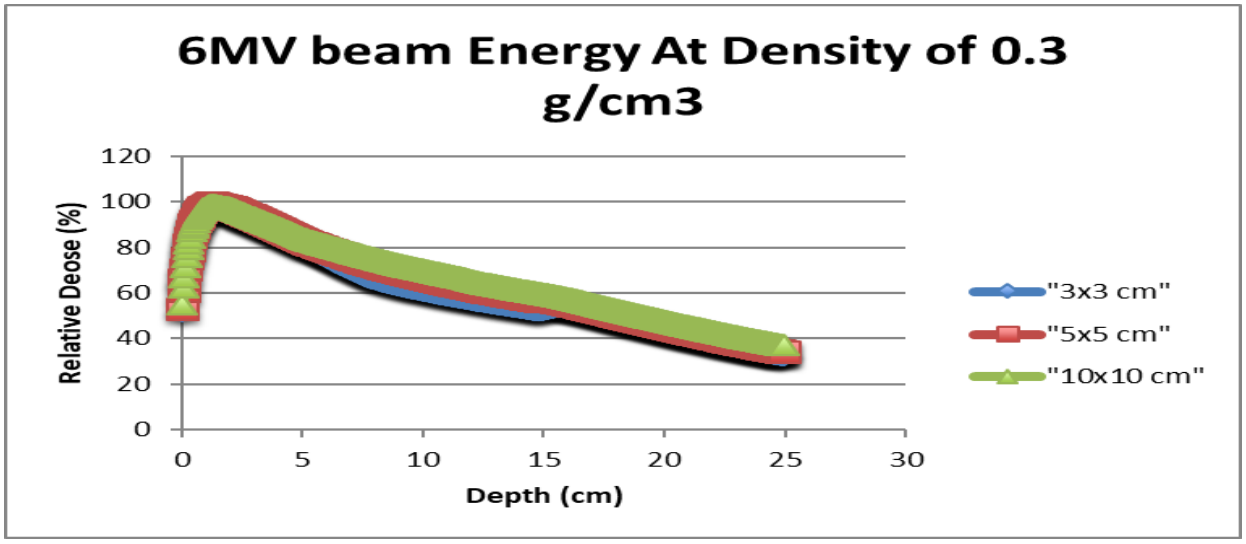

Figure 19 comparing between the different field sizes and beam energy of (6MV) and a Density (0.3g/cm^3).

In figure 20 the relative dose absorbed in percentage against the depth is also shown. The representation for the lung medium is in a depth between 5 cm and 15 cm having a heterogeneous density of 0.3 g/cm3. The Three different field sizes i.e., 3x3 cm, 5x5 cm, and 10x10 cm were irradiated by 10MV and used. The algorithm gives there are different curves for each of the different field sizes. There is no clear impact seen in the 10x10 cm field size, the 5x5 cm field size showed a comparatively small impact, and the 3x3 cm field size showed a large impact of absorption when seen through the lung phantom.

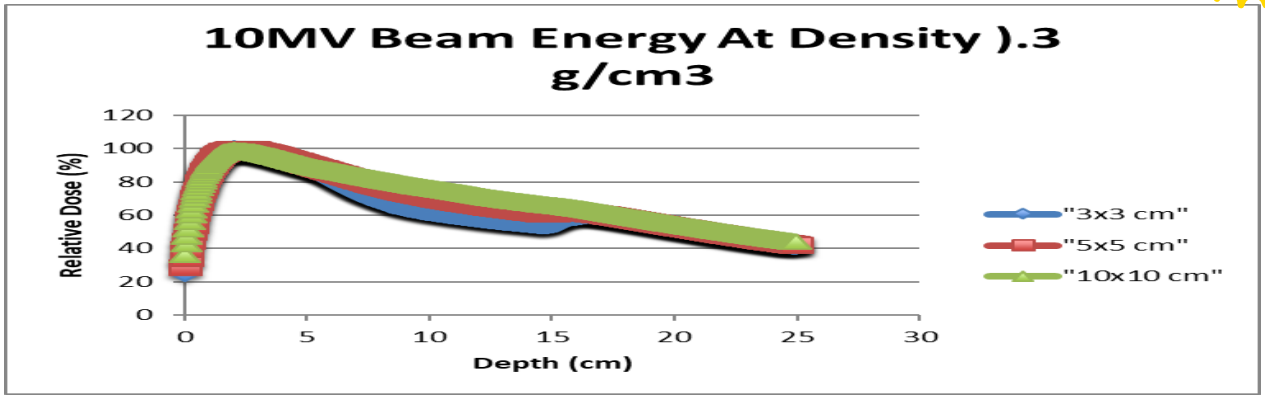

Figure 20 how different field sizes compare when the beam energy (10MV) and density (0.3g/cm3) are the same.

3.5 The Power of Energy

4.5.1 Comparison Between energies being used in the TPS using CCCS

For the comparison of the relative absorption against depths for 6MV pinnacle3 and 10MV pinnacle3 CCCS was used. In Figure 21 it is illustrated that the result obtained from the comparison with constants being the 3x3 cm field size and a heterogeneous density of 0.3 g/cm3. Which can be seen in the figure 4-17, the decrease in dose absorption for 6MV pinnacle3 starts before reaching the lung media that lies in between the depths of 5 cm and 15 cm respectively. The decrease starts at a depth of about 2 cm and continues, but at the end of the lung media, which is about 15 cm in depth, the dose absorption for the 6MV beam energy increased albeit slightly. For the case of 10 MV beam energy, the decrease in the dose absorption started at a depth of about 4 cm with a maximum decrease seen at a depth of 15 cm before rising slightly to a depth of 16, and afterward, it decreased for the remainder of the graph.

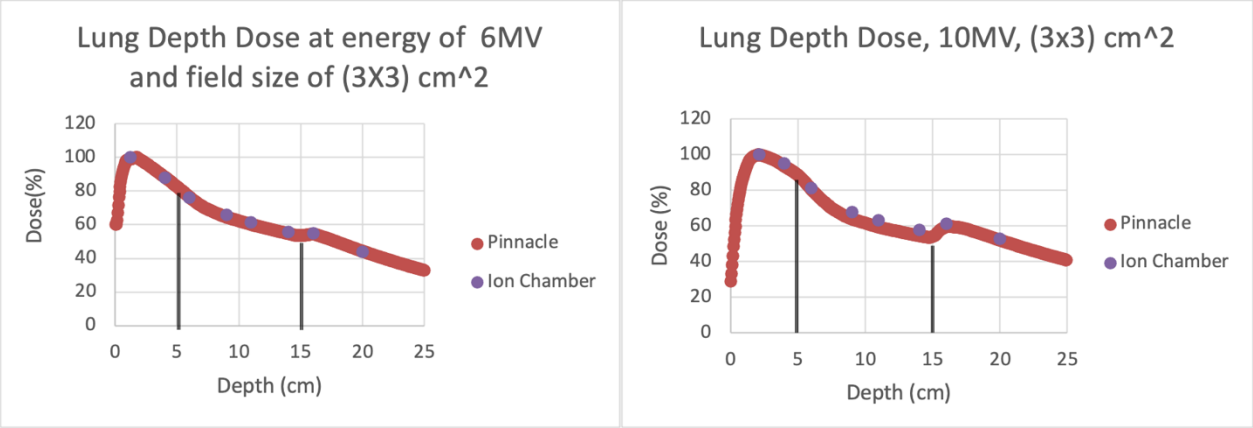

Figure 21 a comparison between two energies 6MV and the 10MV for the same field size of 3cm x 3cm and density of 0.3g/cm^3.

In the given figure 22, the same beam energies of 6MV and 10MV respectively were compared for the same field size of 3x3 cm with the variable being the heterogeneous density of 0.1 g/cm3. From a depth of about 2 cm, the absorption of dose for both the 6MV and 10MV started lowering with the lowest point occurring at the lung medium in between the depth of 5 cm and 15 cm. After reaching the depth of 15 cm the beam energy entered the water medium immediately, the absorption of dose for the two beam energies started increasing up to a depth of 16 cm and after which it declined.

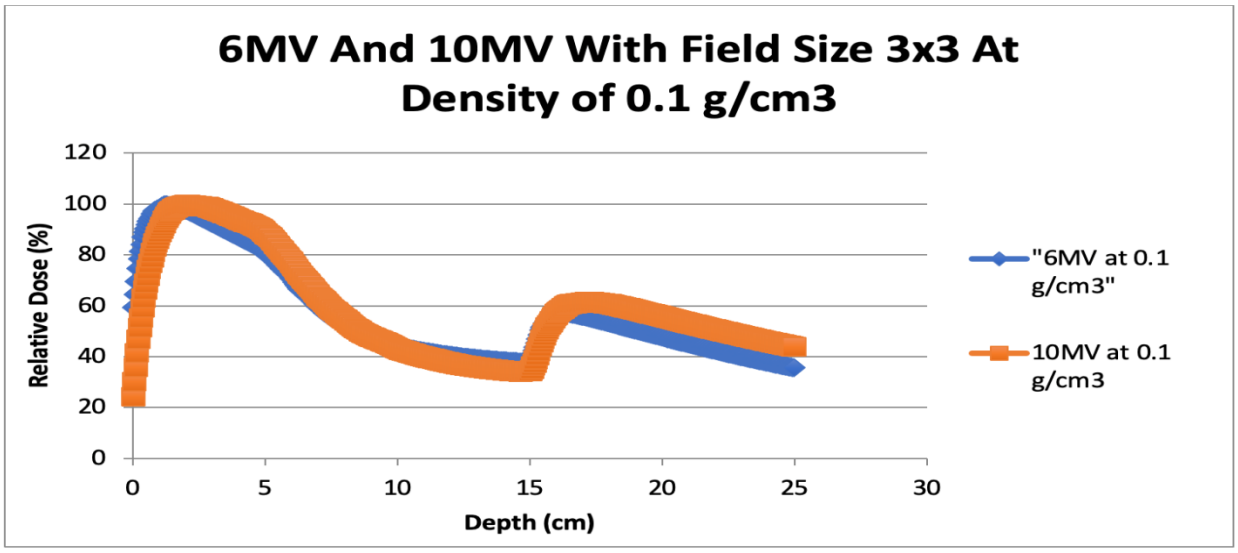

In figures 22, a comparison among the two energies 6MV and 10MV for the same field size 3cm x 3cm and density of 0.1g/cm^{3}is made.

3.5.2 The results of the CCCS and the Ionization Chamber are compared in terms of energy

The comparison made in figure 21 was of a 6MV pinnacle3 being compared against a 10MV pinncle3 and a CCCS at 6MV ionization chamber compared against CCCS at 10MV ionization chamber. The constants in this comparison were the 3x3 cm field size and the heterogeneous density which was of 0.3 g/cm3. The dose absorbed at 6MV pinnacle3 was the same as the absorbed dose found at 6MV ionization chambers. The dose absorbed at 10MV pinnacle3 did not agree with the absorbed dose shown at 10MV of the ionization chamber. Additionally at the beginning, the 10MV ionization chamber was in slight disagreement with the 10MV pinnacle3, which decreased when the beam energy went across the lung medium.

	Pinnacle3			Experimental		
	3x3 cm	5x5 cm	10x10 cm	3x3 cm	5x5 cm	10x10 cm
6MV	60.1	65.1	68.9	61.2	65.4	68.7
10MV	59.4	68.5	75.1	63.0	70.7	75.6

Table1: The percentage of dose absorbed at the nearest depth point towards the middle (10.99cm) in the phantom of the lung via the simulation by Pinnacle3 and the percentage of dose absorbed at nearest depth point towards the middle (11cm) of the lung phantom through the measurements on the ionization chamber.

A depth which was selected to be 10.99cm CCCS as seen in table 1 was used in the algorithm there was a middle point at 11cm CCCS that was applied. The incentive behind using this point was that it lied in the center of the lung phantom and within the heterogeneous density of 0.3g/cm3.

The formula given in the following shows the difference in the dose measurements among the CCCS and the ionization chamber and tabulating the results in table 2

$$\%Dose\ Different = \frac{D_{ion-ch} - D_{conv}}{D_{ion-ch}} \times 100$$

	% Dose difference		
	3x3	5x5	10x10
6MV	1.681675	0.334618	-0.28896
10MV	5.828941	3.026936	0.54621

table -2 The relationship between calculation in the TPS pinnacle3 and the measurements done in ionization chamber from table 1

The percentage dosage variation for beam intensities of 6MV and 10MV was shown in table 2. It can be shown that employing 10MV beam intensity with a field dimension of 3x3 cm resulted in the maximum percentage dose variation of 5.828941 percent, whereas the percentage dose variation for 5x5 cm and 10x10 field dimensions was 3.026936 percent and 0.54621 percent, accordingly. When utilizing 6MV beam intensity, the field area increases but the percentage of dosage variation decreases. A dosage differential of -0.28896 percent was observed at a field dimension of 10x10, 0.334618 percent at a field dimension of 5x5 cm, and 1.681675 percent at a field dimension of 3x3 cm.

4. Discussion

The convolution calculation method was applied in this study for the determination of the radiotherapy radiation dose changes required due to homogeneity density changes seen in the lungs. A comparison was made between this calculation method and the treatment planning system (TPS). The calculation accuracy for the dose CCCS was evaluated by a comparison between the measured and calculated isodose lines for a heterogeneous media of water and lung media [14]. The comparison made between the measured and calculated dose for the symmetric fields showed an average difference of only 3.5%.

This work utilized the following metrics: a radiated beam intensity of 6MV and 10MV, a heterogeneous phantom density of 0.1 g/cm3 for the lung medium, 0.2 g/cm3 for the first water medium, 0.3 g/cm3, and 0.4 g/cm3 for the second water medium. This study also compared the findings of the two-beam intensities' ionization compartments through the medium. The International Commission on Radiation Units (ICRU) accepts a highest of 5% computation errors at a low density of 0.3 g/cm3, narrow field dimensions, and high beam power, while the errors in this research work are within the recommended limits, producing the findings and relative evaluation of the differences reliable. The dosage allocation and assimilation are affected by the variables of beam intensity, density medium, and field dimensions, thus the analysis of the findings obtained centered on the precision of the CCCS with the variables utilized as a baseline [15].

4.1 By using Collapsed Cone Convolution Superposition (CCCS) to calculate the doses.

The variations and the accuracy which is seen in the dose calculation might have been affected by perturbations which are by nature energy and density-dependent, which is why such a trend such as seen in the graphs for low-density medium being the lung medium. To obtain the dosimetry data Pinnacle3 was used for small beams of the photon. The use of an ionization chamber was done in this experiment to check the accuracy of CCCS dose calculation algorithms by having it compared [16]. For the water medium which was the first and lied at the depth of 5cm, the CCCS method relying on pinnacle^3 gave a uniform trend for the energy beams and the heterogeneous densities, when the beam energy reached the lung medium the results given by CCCS were in correspondence for the 10MV beam energy through 5x5 cm and the 10x10 cm field size. This were 3.026936% and 0.54621% respectively which are being less than

the maximum allowed difference which is of 5%. The exceptions that were seen mainly in the 10MV 3x3 cm field sizes of the lung medium having the dose difference of 5.828941% and is shown in table 2 concurrently every one of these differences occurred at the centre of each of the medium. the interface separating one medium to the next, such as, at point 5 cm depth and 16 cm depth in figure 14 and 15, there is an interface error resulting from the differences in attenuation coefficient, the beam energy absorption co-efficient and the collision stopping powers.

One more potential cause for the error can be due to the forward electronic disequilibrium (FED) which occurs due to the generation of electrons on either side of the media is different from each other. The result of such differences is prolapsing leading to errors. For the under prediction of the dose distribution when the 6MV beam of energy was used the error which arose was below the acceptable range at -0.28896% error being recorded at 10x10cm field size, an error of 0.334618% was recorded for the 5x5 cm field size and finally an error of 1.681675% was recorded for the 3x3 cm field size all of which is shown in table 2.

Through the consideration about the absorbed dose percentage and by ignoring the errors that could probably have occurred it is seen that the results of the experiment are much higher than the pinnacle[3] results for the field of 10x10 cm size both for the 6MV and 10MV beam energies. For the field size of 10x10 cm in 10MV the experimental value is low which is an indication that is generally in all the circumstances, the results of the experiment are particularly related to more errors ranging from the human errors to the equipment variations and scaling.

Considering the example in the table 1, the result of the experiment obtained through the ionization chambers were higher than the results acquired from the method of the

CCCS pinnacle^3 except in the 5x5 cm for 10MV in that case it is not observed as an error as it generates a negative percentage of - 0.28896% as revealed in the table 2. Based on these results, it is interpreted that the results from the TPS which makes use of the CCCS dose calculation algorithm provide an accurate result for all the beam energies, the medium density, and the field sizes [17]. The maximum inconsistency among the results of Monte Carlo and Pinnacle^3 is recorded as to be 5.828941% for the 10MV and 3x3 cm field size. It is due to the un-conditional value of the dose that is big therefore this relatively big absolute dose variance directed towards a relatively higher difference in the percentage. Through this analysis, it is seen that the Collapsed Cone Convolution Superposition method (CCCS) is correct, and it is more consistent method for the calculation of the dose absorption through the various media with the heterogeneous densities in comparison with the experimental Monte Carlo methods that comprises of the uses of the ion chambers. Considering for example in the figure 21, a deviation is seen in the results of the results for the 10MV ionization chamber, and it was in total discrepancy with the 10MV and 6MV pinnacle^3 at the low-density medium that is regarded as the lung medium.

4.2 Effects of Density on Dose Distribution

The significant determinant of the rate of dose absorption when the various beam energies are irradiated is the density of the media. The effect of density on the absorption dose absorption will be seen in the figure 5, 6, 7, 8, 9 and 10. It can be seen through the figures and from all the beam energy that is irradiated, that the rate of absorption is decreased at a low medium density that lies among the depths of 5 cm and 15 cm and this reduction is initiated at the boundary of the adjoining media. When the beam energy moves through the interface towards a medium of low density, then it realizes a lateral electronic disequilibrium (LED) that is produced by the

various electron number in the adjacent media. The decrease of the absorption is quick at the medium initiation as compared to that at the exit of the medium where there lie a high range of the secondary electron. There are normally more electrons present at the end of the medium than at the start because of the self-ionization that is produced due to the electron's interaction with the molecules. It is found out from this that the secondary electrons play an important role as regard to the medium's density. Considering for example that at a lower density medium, there exists a larger range of secondary electrons that end up into a lateral electronic disequilibrium (LED) which subsequently results in the decrease of the lung tumor doses that are prescribed in the international research findings.

The beam energies isodose profile for the 10 MV and 6 MV are shown in the Figure 17 and 18. The density of the medium is regarded as a crucial determinant of the dose profile. Considering for example, the increase in the penumbra's width means that the beam energy is in the medium having a low density. When there is a decrease in the penumbra width there is an increase in the density of the medium which means that the density of the medium is contrariwise proportional to the width of penumbra. At the low density, the adjacent motion of the particles that are charged increases with the depth henceforth falling the rate of the absorption of the beam energy into the tissues.

4.3 Effect of Beam Energy on Dose Distribution

The best analyze of the beam energies can be done by making a comparison of 6MV and 10MV and the various heterogeneous densities of 0.3 g/cm^3 and 0.1 g/cm^3 as can be seen in the figure 21 and 22. Once the medium density is integrated in the analysis then the analysis will become more practical. At an assorted density of 0.1 g/cm^3, the

relative dose absorption when the beam energy of 10MV was irradiated is greater than for 6MV in water media but lesser than at 6MV in the lung medium. Considering for example the beam energy was 31.7% for the 10MV at a low density medium and the beam energy was 36.5% for the 6MV at low density medium. It can be explained that the number of the secondary electrons The explanation is that the number of secondary electrons grows in the beam energy which results in the origin of the LED that is accountable for reduction in the doses of the lung tumor. In the case of the high-density medium, the high beam energy is considered as favourable as its immense impact of the energy increases the photons penetration and hence result in increasing the dose that is absorbed as associated to a low beam energy of 6MV. The 6MV is favourable in the case of the low medium as it is of less LED creation and the secondary elector generation and the conclusion of the medium that upsurges the dose absorption rate that exists in the tissues.

It is shown from the figure 21 that when there is a higher beam energy of 10MV, than there exists a higher rate of ionization in the low-density medium. The ionization is also low for a 6MV beam energy at the lung medium. The table 2 provides the absorption of dose when there is a beam energy of 6MV is irradiated under the suitable maximum of 5% but in this case the error is considered slightly outside the recognized limits for the 10MV at 3x3 cm cm field sizes with 5.828941% errors correspondingly. It is indicated through this that the error in dose absorption grows higher with an increase in the beam energy that is provided. Based on the isodose curve comparison provided in the figure 17 and 18, an increase in the beam energy rises the penumbra's girth.

4.4 Field Sizes Have an Impact

In both 19 and 20 figure, the field sizes that are utilized for the purpose of the research are 3x3 cm, 5x5 cm and 10x10 cm which shows that an increase in the size of the field results in an increase in the absorption of the dose once the other factors in the research are not considered. Once more, an increase in the size of the field lead to a decrease in the errors when a 6MV was smeared but a discrepancy existed in the errors once a 10MV was pertained. A decrease in the size of the field goes to a limit where there exists smaller gap, from the meeting point to the closest field edge as associated to the number of electrons(secondary) at the departure in the medium particularly when the LED has arisen. Once the size of field becomes tremendously small, then an importance total dose reduction exists in the phantom.

As represented in figure 19 and 20, for the field sizes of 5x5 cm and 10x10 cm, it becomes convenient to forecast the changes in the relative dose percentages as the two graphs are really close to each other irrespective of the irradiated beam energy. On the other hand, the field size 3x3 cm is comparatively distant from the other field sizes that have an important difference in the forecasting of the percentages of the doses. After this it becomes hard to have a noteworthy comparison when the sizes of the field are less than 3x3 cm are utilized.

4.5 Lung Radiotherapy

A radiotherapy is required for the therapy of lung cancer and its management, all of this is dependent upon the already discussed parameters like the density, the field sizes, and the beam energy of the medium from which the beam energy is irradiated. In particular, the lung density is a regarded as a crucial determinant as reflected by its effects on the sizes of the field, the LED and the secondary electrons that move between the medium. The health and the age of an individual helps in regulating the

lung density and therefore the density generally fluctuates among 0.1 g/cm^3 and 0.4 g/cm^3 and therefore it is termed as heterogeneous density although it is still lower than the water mediums density. It is considered significant to consider all the factors that are the cause of the LED energy and field sizes in advance of resolving to a lung radiotherapy present in a low-density medium. The results that are generated through this experiment will aid one in making a choice about a specific beam energy and the size of the field provided at a given medium density that is based on some other factors. These factors constitute of the health of an individual, the influencing factors to the operations of the radiotherapy and the exposure that was done previously which influence the dosage and therefore regulate the amount of beam energy and field sizes when the density of the lung is decided.

The LED effect increases once there is an increase in the beam energy for example for the 6MV and 10MV and the field sizes of 10x10 cm evidently portray the effect of LED even at the lung density of as low as the 0.1 g/cm^3. It is advised that a 6MV for a field size 5x5 cm could be used for a respective lung density of 0.2 g/cm^3, 0.3 g/cm^3 and 0.4 g/cm^3. It is seen that a respective lung density of 0.1 g/cm^3 may end up into reducing the absorption of the dose present in the lung medium and it may therefore intervene with the absorption of obliged dosage for the lung cancer treatment. It is evident from the figure 6, that the relative dose absorption percentage is as low as 47% at the end of the lung medium and the point depth of 15 cm.

A density of lung of 0.1 g/cm^3 is not considered plausible for beam energy of 6MV having a field size of 3x3 cm as the relative percentage dose immersed could be about the 32% at the end of the lung medium that is in multiple cases lower for most of the radiotherapy in the lungs. As a result, it is proven that the most suited lung density for the objective of radiotherapy is 0.2 g/cm3, 0.3 g/cm3, and 0.4 g/cm3. The

recommended densities fall within the parameters set forth by the American Association of Physicists in Medicine. The field dimension of 3x3 cm has also been shown to be acceptable for preventing the production of LEDs and the progression of the secondary electrons' upper range.

5. Conclusions

It is concluded through this study that the dose absorption that is calculated by utilizing the TPS is based on the CCCS algorithm that provides an accurate result with the help of Monte Carlo Calculations under the circumstances of the heterogeneous media and low-density materials like the lungs. For the higher beam energy of the 10MV and the smaller field size of 3x3 cm, there is a creation of the LED and a higher range of the secondary electron at the end of the lung medium. The extra ionization is the reason for making the curve for the ionization chamber to be at a higher level as related to the other curve for the 10MV at field size 3x3 cm and the density of 0.3 g/cm3.

the density of the lung medium and the beam energy that is provided has an influence on the distribution of the dose. Generally, the dose absorption decreases once the depth increases. The penumbra width increases with an increase in beam energy and the density of the medium decreases. There is an increasing LED effect at 10MV and a secondary electron along with an increase in the width of the penumbra. It is due to this reason that 6MV is considered as the most recommended energy for the beam. There is a need of further work that must be done to regulate the dose absorption when the size of the field is 4x4 cm with a beam energy of 8MV that is utilized for calculating the CCCS, LED, secondary electrons by making use of the Monte Carlo Calculation at various densities.

References

1.Australian Cancer Research Foundation. *How radiation is used to treat lung cancer* (2021).

2.Sholih, Mally G., et al. "Knowledge, attitudes, and practices of lung cancer risk factors in West Bandung Society." *Journal of Pharmacy And Bioallied Sciences* 11.8 (2019): 574.

3. Parashar, Bhupesh, Shruthi Arora, and A. Gabriella Wernicke. "Radiation therapy for early stage lung cancer." *Seminars in interventional radiology*. Vol. 30. No. 02. Thieme Medical Publishers, 2013.

4. Australian Institute of Health and Welfare & Cancer Australia 2011. Lung cancer in Australia: an overview. Cancer series no. 64. Cat. no. CAN 58. Canberra: AIHW.

5. Sholih, Mally Ghinan, et al. "Risk factors of lung cancer in Indonesia: A qualitative study." *J. Adv. Pharm. Educ. Res*| *Apr-Jun* 9.2 (2019): 41-45.

6. Samet, Jonathan M., et al. "Lung cancer in never smokers: clinical epidemiology and environmental risk factors." *Clinical cancer research* 15.18 (2009): 5626-5645.

7.Uzel, Esengül Koçak, Metin Figen, and Ömer Uzel. "Radiotherapy in lung cancer: current and future role." *Sisli Etfal Hastan Tip Bul* 53.4 (2019): 353-60.

8.Rachtan, Jadwiga. "Alcoholic beverages consumption and lung cancer cell types among women in Poland." *Lung Cancer* 35.2 (2002): 119-127.

9. Baumann, Pia, et al. "Outcome in a prospective phase II trial of medically inoperable stage I non–small-cell lung cancer patients treated with stereotactic body radiotherapy." *Journal of Clinical Oncology* 27.20 (2009): 3290-3296.

10.Vinod, Shalini K., and Eric Hau. "Radiotherapy treatment for lung cancer: Current status and future directions." *Respirology* 25 (2020): 61-71.

11.Baker, S., Dahele, M., Lagerwaard, F. J., & Senan, S. (2016). A critical review of recent developments in radiotherapy for non-small cell lung cancer. *Radiation oncology*, *11*, 1-14.

12.Alhassani, Ali, Amitabh Chandra, and Michael E. Chernew. "The Sources of the SGR “Hole”." (2012).

13. Mackie, T. R., J. W. Scrimger, and J. J. Battista. "A convolution method of calculating dose for 15-MV x rays." *Medical physics* 12.2 (1985): 188-196.

14. Estrada Espinosa, Julio Cesar, Segundo Agustín Martínez Ovalle, and Cinthia Kotzian Pereira Benavides. "Dosimetric algorithm to reproduce isodose curves obtained from a LINAC." *Computational and Mathematical Methods in Medicine* 2014 (2014).

15. Dawod, Tamer. "Evaluation of collapsed cone convolution superposition (CCCS) algorithms in prowess treatment planning system for calculating symmetric and asymmetric field size." *Int J Cancer Ther Oncol* 3.2 (2015): 8.

16. Calvo, Oscar I., et al. "On the quantification of the dosimetric accuracy of collapsed cone convolution superposition (CCCS) algorithm for small lung volumes using IMRT." *Journal of applied clinical medical physics* 13.3 (2012): 43-59.

17.El Shahat, K., El Saeid, A., Attalla, E., & Yassin, A. (2014). Comparative Study between Measurement Data and Treatment Planning System (TPS) in Small Fields for High Energy Photon Beams. *International Scholarly Research Notices*, *2014*.